Ca2+ waves coordinate purinergic receptor–evoked integrin activation and polarization

Article

Accepted Version

It is advisable to refer to the publisher's version if you intend to cite from the work. See Guidance on citing.

One-sentence summary: Two distinct P2Y receptors are required for full activation of platelet integrin and fibrinogen binding.

Editor's summary:
Ca²⁺ waves and integrin activation
The integrin GPIIb/IIIa is highly abundant on the surface of platelets and can be activated by intracellular Ca²⁺ signaling in an "inside-out" manner to bind to the adhesive ligand fibrinogen. Bye *et al*. imaged intracellular Ca²⁺ signaling and fibrinogen binding events in primary rat megakaryocytes activated through the ADP-stimulated receptors $P2Y_1$ and $P2Y_{12}$. The authors found that signaling by both receptors was required for full integrin activation, which depended on $P2Y_1$-stimulated Ca²⁺ signaling and $P2Y_{12}$-stimulated activation of the kinase PI3K. In addition, fibrinogen binding became polarized in these cells in a manner dependent on the direction of ADP-stimulated Ca²⁺ waves.

Ca²⁺ waves coordinate purinergic receptor–evoked integrin activation and polarization

Alexander P. Bye,[1][*] Jonathan M. Gibbins,[1] and Martyn P. Mahaut-Smith[2][*]

[1]Institute for Cardiovascular and Metabolic Research, University of Reading, Reading, UK, RG6 6AS. [2]Department of Molecular and Cell Biology, University of Leicester, Leicester, UK, LE1 7RH.

[*]Corresponding author. Email: a.bye@reading.ac.uk (A.P.B.); mpms1@le.ac.uk (M.P.M.-S.)

Abstract

Cells sense extracellular nucleotides through the P2Y class of purinergic G protein–coupled receptors (GPCRs), which stimulate integrin activation through signaling events, including intracellular Ca²⁺ mobilization. We investigated the relationship between P2Y-stimulated repetitive Ca²⁺ waves and fibrinogen binding to the platelet integrin $\alpha_{IIb}\beta_3$ (GPIIb/IIIa) through confocal fluorescence imaging of primary rat megakaryocytes. Costimulation of the receptors $P2Y_1$ and $P2Y_{12}$ generated a series of Ca²⁺ transients that each induced a rapid, discrete increase in fibrinogen binding. The peak and net increase of individual fibrinogen binding events correlated with the Ca²⁺ transient amplitude and frequency, respectively. Using BAPTA loading and selective receptor antagonists, we found that Ca²⁺ mobilization downstream of $P2Y_1$ was essential for ADP-evoked fibrinogen binding, whereas $P2Y_{12}$ and the kinase PI3K were also required for $\alpha_{IIb}\beta_3$

activation and enhanced the number of Ca^{2+} transients. ADP-evoked fibrinogen binding was initially uniform over the cell periphery but subsequently redistributed with a polarity that correlated with the direction of the Ca^{2+} waves. Polarization of $\alpha_{IIb}\beta_3$ may be mediated by the actin cytoskeleton, because surface-bound fibrinogen is highly immobile, and its motility was enhanced by cytoskeletal disruption. In conclusion, spatial and temporal patterns of Ca^{2+} increase enable fine control of $\alpha_{IIb}\beta_3$ activation after cellular stimulation. $P2Y_1$-stimulated Ca^{2+} transients coupled to $\alpha_{IIb}\beta_3$ activation only in the context of $P2Y_{12}$ co-activation, thereby providing an additional temporal mechanism of synergy between these Gq- and Gi-coupled GPCRs.

Introduction

The $\alpha_{IIb}\beta_3$ integrin (GPIIb/IIIa) is one of the most highly expressed platelet surface proteins and has a key role in hemostasis through its ability to bind to several adhesive ligands, particularly fibrinogen and von Willebrand factor (*1*). Blood cell integrins exhibit a low affinity for their ligands under resting conditions; however, "inside-out" activation after adequate cellular signaling induces a conformational change that promotes the high-affinity state and thus ligand binding (*2*). Among the signaling events that couple platelet receptors to $\alpha_{IIb}\beta_3$ integrin activation, cytosolic Ca^{2+} flux plays a crucial role through its ability to stimulate the Ca^{2+}-sensor CalDAG-GEFI and thus also the small G protein Rap1 (*3, 4*). Sufficient activation of Rap1 promotes the binding of talin to $\alpha_{IIb}\beta_3$ to shift the integrin into its high-affinity state (*5-8*). However, GTP loading of Rap1 by CalDAG-GEFI is opposed by the constitutive GAP activity of RASA3; thus, $\alpha_{IIb}\beta_3$ integrin activation downstream of phospholipase-C (PLC)-coupled receptors is limited unless accompanied by phosphoinositide 3-kinase (PI3K)-induced inhibition of RASA3, for example after stimulation of $G\alpha_i$-coupled $P2Y_{12}$ receptors (*5*).

Intracellular Ca^{2+} responses do not occur as uniform increases throughout the cytoplasm, but instead display complex spatiotemporal patterns in the form of restricted punctate events, oscillations, and waves (*9, 10*). Several studies have demonstrated the functional relevance of the spatial and temporal information within these cytosolic Ca^{2+} increases. For example, the frequency of oscillations determines both the efficiency and specificity of gene transcription in lymphocytes (*11*), and unitary Ca^{2+} events can play different roles compared to those of global Ca^{2+} increases during smooth muscle contraction (*12*). Ca^{2+} waves promote intracellular signaling over a long distance in large cells (*13-15*) and coordinate certain types of cardiac myocyte contraction (*16*). In the platelet, Ca^{2+} transients triggered by environmental stimuli induce procoagulant activity (*17, 18*) in a manner that is dependent upon the Ca^{2+} spiking pattern of the individual cell (*19, 20*). However, the relationship between the spatiotemporal patterns of cytosolic Ca^{2+} signals and inside-out integrin activation is unclear.

Previous reports have raised concerns that cell culture systems do not fully reproduce the events underlying agonist-evoked integrin activation in highly specialized cells such as platelets (*21*). Here, we used freshly isolated megakaryocytes (MKs) as a primary cell type that displays repetitive Ca^{2+} waves (*22, 23*) and robust inside-out activation of the $\alpha_{IIb}\beta_3$ integrin (*24, 25*) to investigate the interaction between these two events. We showed that transient Ca^{2+} waves downstream of $P2Y_1$ receptors coupled to $\alpha_{IIb}\beta_3$ activation within seconds, but only when $P2Y_{12}$ receptors were co-stimulated. The extent of fibrinogen binding was dependent upon both the amplitude and interval of the Ca^{2+} transient. Although ionophore-generated, sustained Ca^{2+}

increases alone activated the integrin, this occurred with a substantial delay. Thus, the acceleration of Ca^{2+}-dependent inside-out $\alpha_{IIb}\beta_3$ activation by $P2Y_{12}$ receptors represents a key component of the synergy between Gq- and Gi-coupled P2Y receptors. We also provide evidence that the net direction of the ADP-evoked Ca^{2+} waves may explain the polarization of fibrinogen binding observed during the later stages of this functional response.

Results

P2Y-evoked Ca^{2+} transients mediate precise temporal activation of $\alpha_{IIb}\beta_3$

To investigate the relationship between intracellular Ca^{2+} and $\alpha_{IIb}\beta_3$ activation, primary rat MKs were exposed to a hydrolysis-resistant ligand of both $P2Y_1$ and $P2Y_{12}$ receptors, ADPβS, which avoids the loss of agonist due to ectonucleotidase activity in Ca^{2+}-containing external saline (26). ADPβS evoked a series of transient increases in whole-cell intracellular Ca^{2+} and stimulated fibrinogen binding at the plasma membrane, which served as a marker for activation of the integrin $\alpha_{IIb}\beta_3$ (Fig. 1A and movie S1). Peripheral fibrinogen binding increased in a stepwise manner that coincided with the occurrence of $[Ca^{2+}]_i$ transients (Fig. 1B). Upon closer analysis, a discrete increase in fibrinogen binding (Fig. 1C) was found to follow each $[Ca^{2+}]_i$ transient (Fig. 1D). It was therefore possible to quantify the properties of each $\alpha_{IIb}\beta_3$ activation event in terms of the peak increase in fibrinogen binding (Peak ΔF) and the net change in fibrinogen binding between successive $[Ca^{2+}]_i$ transients (Net ΔF). We also quantified the peak of each $[Ca^{2+}]_i$ transient (Peak $\Delta F/F_0$) and the interval between transients. Correlation was observed between the maximum increase in fibrinogen binding (Peak ΔF) and the peak increase in Ca^{2+} (Peak $\Delta F/F_0$) in 91% of MKs (Fig. 1E). This indicates that the amplitude of the Ca^{2+} transient determines the

magnitude of $\alpha_{IIb}\beta_3$ activation. A statistically significant correlation was also observed between the net change in bound fibrinogen at the end of the period between successive Ca^{2+} transients (Net ΔF) and the interval of the Ca^{2+} transient in 75% of MKs (Fig. 1F). This further suggests that the frequency of Ca^{2+} transients determines whether a net accumulation or reduction in the amount of activated, fibrinogen-bound integrin $\alpha_{IIb}\beta_3$ occurs between successive Ca^{2+} transients. The gradient describing this relationship was not statistically significantly different between individual MKs (mean value: $-1.28\Delta Fs^{-1} \pm 0.518$). The x-intercept, which reflects the inter-transient interval below which the net fibrinogen binding switches from an increase to a decrease, varied between different cells (range: 12 to 44 s) as expected from the intercellular heterogeneity in the magnitude of the Ca^{2+} responses and thus also the fibrinogen-binding events. Together, these data suggest that Ca^{2+} transients promote both the immediate and the cumulative activation of $\alpha_{IIb}\beta_3$ through both their amplitude and frequency of occurrence.

P2Y$_1$-dependent repetitive Ca^{2+} increases stimulate $\alpha_{IIb}\beta_3$ activation only in combination with P2Y$_{12}$-dependent signaling

Individual Ca^{2+} transients evoked by P2Y receptors stimulated a finite increase in integrin $\alpha_{IIb}\beta_3$ activation after a mean delay of 2.9 ± 0.75 s [measured from initiation of the $[Ca^{2+}]_i$ transient to the onset of fibrinogen binding; (Fig. 2, A and B)]. Loading of MKs with the Ca^{2+} chelator BAPTA to an extent sufficient to prevent a detectable ADPβS-evoked Ca^{2+} increase abolished the fibrinogen binding event (Fig. 2C). This confirms previous evidence that increased $[Ca^{2+}]_i$ is an essential component of the P2Y receptor signaling events leading to integrin $\alpha_{IIb}\beta_3$ activation (*27, 28*). Overlay of the integral of the $[Ca^{2+}]_i$ increase further highlighted the close association of this

cytosolic signal with subsequent integrin activation and the consistent lag between the two events across multiple transients (Fig. 2D).

ADP stimulates two receptors in platelets, P2Y1 and P2Y12, which couple to Gq and Gi, respectively (*29-35*). The selective P2Y1 antagonist MRS2179 ablated both ADPβS-evoked Ca^{2+} signaling and integrin $\alpha_{IIb}\beta_3$ activation (Fig. 2E). In contrast, ADPβS still stimulated a Ca^{2+} response in the presence of a maximal concentration of the P2Y12 antagonist, Cangrelor, although fibrinogen binding was similarly abolished (Fig. 2F). Thus, signaling downstream of both P2Y1 and P2Y12 is required for activation of integrin $\alpha_{IIb}\beta_3$ by ADPβS in the rat MK, as was previously observed in platelets and murine MKs (*25, 26, 30-33, 35, 36*). The number of Ca^{2+} transients was reduced from 22 per 9-minute period in control settings to only 1 to 3 transients per recording after blockade of P2Y12 receptors, indicating the ability for this Gi-coupled receptor to prolong the Ca^{2+} response. A direct enhancement of a sustained $[Ca^{2+}]_i$ increase in response to the ionophore ionomycin also induced peripheral fibrinogen binding (Fig. 2G and movie S2). This indicates that a prolonged increased amount of intracellular Ca^{2+} stimulates inside-out activation of $\alpha_{IIb}\beta_3$, consistent with a previous study of platelet aggregation (*37*). However, despite stimulating a larger peak Ca^{2+} increase than that observed in response to ADPβS (Fig. 2A), the ionomycin-evoked fibrinogen binding occurred with a statistically significantly greater delay compared to P2Y receptor stimulation (23.6 ± 12.3 s vs 2.9 ± 0.75 s after the initial Ca^{2+} increase, respectively, Fig. 2H). In addition, stimulation of P2Y12 with ADPβS together with ionomycin under conditions of P2Y1 receptor blockade with MRS 2179 (Fig. 2I) had no statistically significant effect on the rate of onset of $\alpha_{IIb}\beta_3$ activation compared to that in response to ionomycin alone

(Fig. 2J). This suggests that an additional signal downstream of P2Y1 or a difference between the spatiotemporal pattern of the ADP-evoked versus the ionomycin-stimulated Ca^{2+} increase contributes to the ability of this Gq-coupled receptor to synergize with P2Y12 in the acceleration of $\alpha_{IIb}\beta_3$ activation.

Synergy between Ca^{2+} transients and PI3K signaling is required for the activation of $\alpha_{IIb}\beta_3$

We next explored the mechanism responsible for temporal synergy between P2Y1 and P2Y12 during ADP-dependent $\alpha_{IIb}\beta_3$ activation in experiments with pharmacological inhibitors of signaling events downstream of these receptors. In MKs and platelets, the Gq-coupled P2Y1 receptor is required for the Ca^{2+} response through its coupling to phospholipase-C (PLC) and thus stimulation of IP_3-dependent Ca^{2+} mobilization (*25, 29, 33*). We found that both the $[Ca^{2+}]_i$ increase and the fibrinogen binding evoked by ADPβS (Fig. 3A) were ablated by incubation with the PLC inhibitor U73122, whereas the structurally related, non-PLC inhibiting analog U73343 had no effect (Fig. 3, B and C). P2Y1 receptors also release diacylglycerol (DAG) and thus stimulate protein kinase C (PKC); however, the pan-PKC inhibitor GF109203 had no effect on ADPβS-stimulated fibrinogen binding (Fig. 3D). GF109203 modified the Ca^{2+} response by preventing its return to baseline between $[Ca^{2+}]_i$ transients, which is likely a consequence of the role of PKC in mediating P2Y1 receptor desensitization and internalization (*38, 39*). The ability of P2Y12 receptors to modulate the P2Y1-dependent Ca^{2+} response has been suggested previously to be mediated through activation of PI3K and also inhibition of adenylyl cyclase (AC), although amplification of $[Ca^{2+}]_i$ by AC inhibition requires co-stimulation of Gs-coupled receptors (*40, 41*). Roles for both PI3Kβ and PI3Kγ in P2Y12-mediated integrin activation have been demonstrated

using both pharmacological tools and isoform-specific knockout mice (*30, 42*). Consistent with these previous observations, we found that the pan-PI3K inhibitor LY294002 mimicked the action of Cangrelor by abolishing the fibrinogen response (Fig. 3E), confirming the crucial role for PI3K in P2Y12-evoked integrin $\alpha_{IIb}\beta_3$ activation (*43-45*). LY294002 also limited the Ca^{2+} response to only 1 to 2 transients. In contrast, inhibition of AC with SQ22536 did not enhance the ADP-evoked Ca^{2+} response (Fig. 3F) or rescue it in the presence of Cangrelor (Fig. 3, G and H). Because PI3K proved critical for ADPβS-evoked activation of $\alpha_{IIb}\beta_3$, we treated MKs with LY294002 before stimulation with ionomycin and found that fibrinogen binding still occurred but only after a statistically significantly increased delay (235 ± 96 s) relative to that in vehicle-treated MKs (Fig. 3I). This effect can be explained by an ability of ionophore-induced $[Ca^{2+}]_i$ increases to directly activate PI3K (*46*). Ionomycin-induced fibrinogen binding was totally abolished by the PLC inhibitor U73122 (Fig. 3J), but not by the control analog U73343 (Fig. 3K), which is consistent with the reported ability of a large sustained $[Ca^{2+}]_i$ increase to activate this Gq-coupled enzyme in platelets (*47*). Together, these results indicate a nonredundant role for PLC in the pathways leading to $\alpha_{IIb}\beta_3$ activation, consistent with effects observed in patients with a platelet-specific deficiency in PLCβ (*48-50*).

P2Y-evoked Ca^{2+} waves promote spatial reorganization of activated $\alpha_{IIb}\beta_3$

In primary MKs, the transient Ca^{2+} increases occurred as waves that traveled across the cytosol (*22, 23*) and had a clear point of origin and direction of travel (Fig. 4A). Because $[Ca^{2+}]_i$ transients are critical in determining the temporal pattern of $\alpha_{IIb}\beta_3$ activation, we investigated whether the waves also modulated the spatial characteristics of fibrinogen binding. The net direction of the

Ca^{2+} waves in each cell was analyzed by calculating a Ca^{2+} polarity score. A value of 1 represents an MK in which all of the Ca^{2+} waves travelled in the same direction, whereas a score of 0 represents an MK in which there was no net dominant directionality. We generated images of the first ten Ca^{2+} waves as well as the radar plots to illustrate the percentage of waves travelling in each direction throughout a recording for a cell with a low Ca^{2+} polarity score (Fig. 4, B and C) and for a cell with a high score (Fig. 4, D and E). Heterogeneity in different MKs was observed in the Ca^{2+} polarity score, which ranged from 0.73 to 0.08 (Fig. 4F).

During the initial 1 to 2 min of a recording, P2Y receptor-evoked fibrinogen binding was distributed evenly around the plasma membrane of the MK. However, in many recordings, the pattern of fibrinogen binding then progressively shifted toward one side of the cell (Fig. 5A). This behavior was not observed after stimulation with ionomycin, which induced a non-waveform, sustained [Ca^{2+}]$_i$ increase and an even distribution of bound fibrinogen around the periphery of the MK throughout the duration of the experiment (Fig. 5B). Development of fibrinogen polarity was analyzed by calculating a fibrinogen polarity score for each MK. A score of 1 represents a MK in which 100% of the fibrinogen bound to one 120° sector of the cell surface, whereas a value of 0 indicates that the fibrinogen is evenly distributed over the membrane surface. Development of polarity peaked approximately 6 min after stimulation with ADPβS (Fig. 5C). As observed for the net direction of the Ca^{2+} waves, ADPβS-evoked fibrinogen binding polarity scores displayed marked heterogeneity, ranging from 0.08 to 0.73 (Fig. 5D). Despite the heterogeneity, the average fibrinogen polarity score for ADPβS (mean: 0.34 ± 0.24) was statistically significantly

higher than that observed in response to ionomycin, which induced a consistently low value (mean = 0.15 ± 0.07).

After stimulation with ADPβS, MKs with low Ca^{2+} polarity scores retained a uniform distribution of fibrinogen binding at their periphery (Fig. 6, A to C). In contrast, MKs with a high Ca^{2+} polarity score displayed a shift in their fibrinogen binding towards one hemisphere (Fig. 6, D to F). Linear regression analysis of the Ca^{2+} and fibrinogen polarity scores confirmed a statistically significant positive correlation (gradient = 0.6; $P < 0.001$) between these two parameters (Fig. 6G). For strongly polarized MKs (fibrinogen polarity scores > 0.5), the average point of origin of Ca^{2+} waves coincided with the side of the cell displaying the center of fibrinogen polarity [mean difference of 18 ± 5.6° between the origin of the $[Ca^{2+}]_i$ waves and the center of fibrinogen polarity (Fig. 6H)]. This indicates that the side of the MK from which most of the $[Ca^{2+}]_i$ waves originated was also the location at which fibrinogen accumulated.

Mobility and reorganization of activated $\alpha_{IIb}\beta_3$ depends on its association with the actin cytoskeleton

Inside-out activation of integrins such as $\alpha_{IIb}\beta_3$ causes association with the actin cytoskeleton through talin (51-54), which limits the mobility of these adhesive receptors within the plasma membrane (55). If $\alpha_{IIb}\beta_3$ is unable to diffuse freely, cytoskeletal reorganization might form part of the mechanism underpinning the development of its polarized distribution. We therefore investigated the diffusive properties of activated $\alpha_{IIb}\beta_3$ using fluorescence recovery after photobleaching (FRAP) of Alexa Fluor 647–labelled fibrinogen bound to the plasma membrane 4

min after stimulation with ADPβS (Fig. 7A). The fluorescence recovered to only 24 ± 7.5% of pre-bleached levels by the end of the 220-s recording (Fig. 7, B and C), suggesting that most of th $\alpha_{IIb}\beta_3$ receptors were immobile within the plasma membrane. Thus, diffusion of the integrin is unlikely to be an important factor in the development of polarity. To test whether the association of $\alpha_{IIb}\beta_3$ with the cytoskeleton limited its mobility, we repeated the FRAP measurements after treatment with cytochalasin D, an inhibitor of actin polymerization (Fig. 7, B and C). Diffusion of bound fibrinogen was statistically significantly increased by cytochalasin D treatment (mean recovery = 36 ± 13%), suggesting that the actin cytoskeleton has a role in limiting the plasma membrane mobility of activated $\alpha_{IIb}\beta_3$ and that major changes in $\alpha_{IIb}\beta_3$ localization are likely to occur only through reorganization of the actin cytoskeleton.

To further investigate the relationship between activated $\alpha_{IIb}\beta_3$ and the actin cytoskeleton, MKs stimulated with ADPβS for 4 min in the presence of Alexa Fluor 647–labeled fibrinogen were fixed and stained with Alexa Fluor 488–conjugated phalloidin. Confocal z-stack images showed that MKs without polarized fibrinogen binding also lacked polarization of actin structure in three dimensions (Fig. 7, D and E). In contrast, MKs in which the bound fibrinogen shifted to one side of the cell also displayed an increase in actin abundance in the same cellular hemisphere (Fig. 7, F and G). These data suggest that repetitive $[Ca^{2+}]_i$ waves can drive directional reorganization of actin, leading to spatial redistribution of activated integrin $\alpha_{IIb}\beta_3$ at the cell surface.

Discussion

Regulation of integrin affinity, referred to as "inside-out" signaling, enables cells to control their interactions with the extracellular environment. Inside-out signaling is a process common to all integrins and involves a conformational change triggered by intracellular events that results in exposure of high-affinity sites for ligand binding. $\alpha_{IIb}\beta_3$ has long served as a model for the cellular regulation of integrins and is highly abundant in platelets and their precursor cell, the MK. Although the critical events that underpin receptor-evoked $\alpha_{IIb}\beta_3$ activation are well-established, the temporal regulation of inside-out signaling has not been explored in detail. Rapid activation of integrins is likely to be important in a number of contexts, not least under the dynamic conditions present in the circulation where the platelet must activate $\alpha_{IIb}\beta_3$ quickly enough to enable adhesion at sites of vascular injury. Primary MKs express functional $\alpha_{IIb}\beta_3$ that undergoes inside out activation upon stimulation with ADP (*24, 25*) and, unlike in the diminutive platelet, it is possible to discern the quantal increase in integrin activation triggered by individual Ca^{2+} transients (Fig. 1). This has enabled us to dissect the temporal relationship between Ca^{2+} signaling events and integrin activation in detail.

We found that the activation of $\alpha_{IIb}\beta_3$ was efficiently induced by individual cytosolic Ca^{2+} transients after co-stimulation of the ADP receptors P2Y1 and P2Y12. Two characteristics of repetitive Ca^{2+} transients were found to control the overall rate of integrin activation. First, the amplitude of the whole-cell Ca^{2+} transient determined the magnitude of the increase in integrin $\alpha_{IIb}\beta_3$ activation after each transient. Second, due to constitutive deactivation of the integrin, the net change in integrin activation over time was controlled by the frequency of the Ca^{2+} transients. Another example of a downstream functional event that is controlled by the amplitude and

frequency of Ca^{2+} transients is lymphocyte gene transcription (*11, 56*). Lymphocyte transcription factors are regulated differentially by the precise characteristics of Ca^{2+} oscillations and provide a basis for the selective stimulation of individual gene regulation pathways downstream of a single second messenger. Several studies showed that the pattern of Ca^{2+} increase in platelets can be specific to individual agonists (*57-59*) and the relationship between Ca^{2+} transients and integrin activation described in the present study may therefore represent a mechanism whereby different agonist species activate integrins with varying levels of efficiency. In addition, because the frequency of Ca^{2+} oscillations in rat MKs increases with agonist concentration (*60*), this provides a mechanism whereby the extent of inside-out activation can be controlled by stimulus strength.

Although we found evidence that integrin activation and fibrinogen binding were reversible, the rate of release was much slower than that of binding, resulting in the accumulation of bound fibrinogen even at low Ca^{2+} transient frequencies. As a result, the pattern of fibrinogen binding bore a strong resemblance to the cumulative Ca^{2+} signal, suggesting that the accumulation of Ca^{2+}-activated intracellular signaling molecules supports inside-out activation. In other cell types, transient Ca^{2+} signaling events are "memorized" by Ca^{2+}-sensing signaling molecules that are rapidly activated but slowly deactivated (*61*). For example, in T-cells, the Ca^{2+}-calmodulin–dependent phosphatase calcineurin is activated by Ca^{2+} transients and subsequently dephosphorylates the transcriptional regulator NFAT, enabling its translocation to the nucleus (*11*). Deactivation of NFAT by phosphorylation occurs slowly, such that the interval between Ca^{2+} transients controls the accumulation or loss of nuclear NFAT, resulting in a pattern that is highly

reminiscent of integrin activation by Ca^{2+} transients in the MK. In platelets and MKs, the Ca^{2+}-sensing molecule CalDAGGEFI mediates the activation of Rap1, which in turn mediates integrin activation (*3*). Rap1 is inactivated by the GTPase-activating protein (GAP) RASA3 (*62*), and it is possible that the interplay between CalDAGGEFI, Rap1, and RASA3 regulates integrin activation in response to Ca^{2+} transients in a manner analogous to NFAT regulation in T-cells.

The two ADP receptors expressed in MKs and platelets, P2Y1 and P2Y12, regulate different halves of the CalDAGGEFI-RASA3 axis that controls Rap1 activity. We exploited this by using receptor antagonists to explore the regulatory roles of P2Y1 and P2Y12 alone and in combination. The Gq-coupled P2Y1 receptor stimulates activation of PLCβ and Ca^{2+} transients that switch on the GTP-exchange activity of CalDAGGEFI, thereby promoting activation of the Ras-like small GTPase Rap1 (*3, 4*). Inside-out $\alpha_{IIb}\beta_3$ activation by ADP also requires co-activation of P2Y12-induced signals (Fig. 2) (*34, 63*). Although this Gi-coupled receptor is linked to the inhibition of AC and the activation of Akt, the crucial P2Y12 signaling event is the inactivation of RASA3 GAP activity that tonically limits GTP-loading of Rap1 (*5*). RASA3 inactivation is induced by P2Y12-evoked PI3K activation, which is why LY294002 mimics the inhibitory effect of P2Y12 antagonists on ADP-evoked fibrinogen binding and Ca^{2+} responses (Figs. 2F and 3E) (*44*). Whereas Rap1 and RASA3 are already predominantly located at the plasma membrane (*7, 64, 65*), CalDAGGEFI and talin require translocation to the cell membrane during inside-out activation of $\alpha_{IIb}\beta_3$ (*66-68*), which could therefore account for a substantial portion of the delay between the Ca^{2+} transients and integrin activation that we observed (Fig. 2). Although P2Y12 antagonists completely blocked the ADP-induced activation of $\alpha_{IIb}\beta_3$ even in the continued presence of Ca^{2+} transients, substantial

fibrinogen binding was observed after the induction of a prolonged Ca^{2+} increase with ionomycin. This is consistent with the ability of the Ca^{2+} ionophore to induce Rap1 activation in platelets (*69*) and indicates that sustained CalDAGGEFI activation can overcome tonic RASA3 activity, although there remains a contribution from PI3K activation (Fig. 3I). However, the effect of an $[Ca^{2+}]_i$ increase alone on fibrinogen binding occurred with a marked delay compared to that observed after ADP-evoked Ca^{2+} transients during P2Y1 and P2Y12 co-stimulation. Indeed, the delay after ionomycin-induced Ca^{2+} increases (23.9 s) was longer than the duration of individual ADP-evoked Ca^{2+} transients (2.5 to 3 s). Thus, the synergy between CalDAGGEFI and RASA3 in promoting Rap1 activity enables brief Ca^{2+} transients to stimulate a discrete increase in integrin activation.

Preventing excessive and toxic activation of Ca^{2+}-dependent proteins (*70, 71*) is envisaged to be one advantage of repetitive transients over sustained increases in this ubiquitous second messenger and thus is a further advantage of the P2Y1-P2Y12 synergy occurring at the level of Rap1 activation. We noted that rapid fibrinogen binding was not observed after co-stimulation of cells through P2Y12 and ionomycin, which suggests that either a difference between the Ca^{2+} increases evoked by P2Y1 and ionomycin or an additional signal downstream of the Gq-coupled receptor accelerates Rap1 activation alongside PI3K activation. However, PKC activation was not involved (Fig. 3D), consistent with the lack of a role for DAG in CalDAGGEFI activation (*72, 73*). Furthermore, inhibition of PLC mimicked the effect of BAPTA-loading; thus, possibilities for the missing signal include IP_3 formation or a decrease in PIP_2 abundance, which requires further investigation.

As previously observed in the MK (*23*), each P2Y-evoked Ca^{2+} transient was initiated at one edge of the cell and spread as a wave across the remainder of the cytoplasm before declining to resting levels. A higher density or greater sensitivity of IP_3 receptors at the site of origin of the wave has been suggested to account for the point of initiation, which then evokes Ca^{2+}-induced Ca^{2+} release through nearby IP_3 receptors, resulting in a spread of the cytosolic Ca^{2+} increase across the cell (*23, 74*). In the MK, the wave origin has a predominant juxtanuclear location (*23*) and, together with previous observations that the polyploidic nucleus is predominantly located in one hemisphere of the cell (*23*), provides the basis for the polarity of the Ca^{2+} signal relative to the cell structure. Thus, the dependence of the fibrinogen binding on the direction of the Ca^{2+} wave could serve as a signal for directional migration of the MK to the sinusoidal blood vessels where proplatelet extension are projected across the vascular endothelium enabling release of new platelets into the circulation, for which polarization is critical (*75*). Indeed, polarized regulation of the small GTPases Cdc42 and RhoA stimulates the GPIb-dependent transendothelial migration of MKs into the circulation (*76*). Furthermore, deletion of the two main platelet isoforms of Rap1 causes reduced proplatelet formation and thus macrothrombocytopenia (*77*).

In conclusion, here, we examined the relationship between spatiotemporal increases in intracellular Ca^{2+} and activation of high-affinity fibrinogen binding sites of the most prevalent platelet integrin, $α_{IIb}β_3$. The work demonstrates that synergy between P2Y1 and P2Y12 receptors accelerates Ca^{2+}-dependent inside-out activation of $α_{IIb}β_3$ to enable individual P2Y1-evoked transient Ca^{2+} waves to stimulate discrete increases in fibrinogen binding. Spatiotemporal

information encoded within the repetitive Ca^{2+} waves determined the extent of fibrinogen binding and also redistribution of the active integrin within the cell membrane.

Materials and Methods

Preparation of rat bone marrow megakaryocytes

Rat bone marrow was extracted from the tibia and femurs of adult male Wistar rats weighing between 300 and 400g. Rats were killed by cervical dislocation in accordance with Home Office license regulations and the University of Leicester Home Office certificate of designation. The femurs and tibia were isolated, the epiphyses removed, and the marrow was then flushed out with 1 ml of Hanks' Balanced Salt Solution (HBSS).

Simultaneous fluorescence imaging of $[Ca^{2+}]_i$ and fibrinogen binding in primary rat MKs

A bone marrow suspension was diluted 10-fold in HBSS (with 1.26 mM $CaCl_2$) containing 2 µM Fluo-3 AM and 0.02% Pluronic F127, incubated for 1 hour at room temperature with gentle agitation, pelleted by centrifugation at 200g, and resupended in HBSS. Alexa Fluor 647–labelled fibrinogen (centrifuged at 13,600 g for 10 min to remove precipitates) was added at a final concentration of 60 µg/ml. MKs were identified by their uniquely large size (diameter >25 µm) and multilobular nucleus (78) and were imaged with an Olympus IX81 inverted confocal laser scanning microscope (Olympus, UK) and a 60x oil immersion 1.35 NA UPLSAPO objective. Cells were mounted in a 200-µl volume chamber (Digitimer Ltd, Welwyn Garden City, UK) in a stable "Z" temperature-regulated holder (Bioptechs Inc, Butler, PA) set to 25°C. Images were captured at 5.4 Hz with a 6X digital zoom at a resolution of 128 x 128 pixels for a total of 9 min. MKs were

preincubated for 10 min with MRS2179 (100µM), Cangrelor (1µM), LY294002 (50µM), SQ 22536 (30µM), U73343 (10µM), U73122 (10µM), or GF109203 (10µM) as described in the figure legends. MKs were incubated with 10 µM BAPTA-AM for 60 min to chelate intracellular Ca^{2+} in some experiments as described. Stimulation with 100 µM ADPβS or 1 µM ionomycin was achieved by direct addition of these compounds to the chamber with an air-displacement pipette held in position by a retort stand.

Solutions and chemicals

Hanks' Balanced Salt Solution (HBSS) contained 1.26 mM $CaCl_2$, 0.493 mM $MgCl_2$, 0.407 mM $MgSO_4$, 5.33 mM KCl, 0.441 mM KH_2PO_4, 4.17mM $NaHCO_3$, 137.93 mM NaCl, 0.338 mM Na_2HPO_4, 5.56 mM D-glucose, 5 mM HEPES (pH 7.35) with NaOH. Pluronic F127, MRS2179, cytochalasin D, LY294002, formyl saline, and ADPβS were obtained from Sigma-Aldrich (Gillingham, UK). Fluo-3 AM, Alex Fluor 488–conjugated phalloidin and Alexa Fluor 647–conjugated fibrinogen were from Invitrogen (Paisley, UK). SQ 22536, U73343, and U73122 were from Tocris Bioscience (Bristol, UK). Cangrelor was a kind gift from AstraZeneca (Moindal, Sweden).

Temporal analysis of whole-cell Ca^{2+} increases and fibrinogen binding

Temporal changes in intracellular Ca^{2+} and fibrinogen binding across the entire cell were analyzed with ImageJ software (Rasband, W.S., ImageJ, U. S. National Institutes of Health, Bethesda, Maryland, USA, https://imagej.nih.gov/ij/, 1997-2016). Mean fluorescence intensity values were measured within a circular region of interest (ROI) containing the entire MK. Background-subtracted Fluo 3 fluorescence values (F) were converted to F/F_0 ratios to normalize for the

amount of fluorescence before the addition of agonist (F_0). Increases in Alexa Fluor 647–conjugated fibrinogen fluorescence are expressed as the change in signal above that under pre-stimulated conditions ($F-F_0$).

Calculation of Ca^{2+} wave and fibrinogen binding polarity scores

Ca^{2+} wave direction was assigned to one of eight directions (representing 45º sectors of the MK) and used to calculate the average wave direction and magnitude (Ca^{2+} polarity score) using vector analysis similar to that used to calculate average wind direction and speed (*79*). The following equations were used for the vector analysis:

Equation 1:

$$\vec{u} = -u_i \times \sin\left[2\pi \times \frac{\theta_i}{360}\right]$$

Equation 2:

$$\vec{v} = -u_i \times \cos\left[2\pi \times \frac{\theta_i}{360}\right]$$

Equation 3:

$$Ca^{2+} Polarisation\ Score = (\vec{u}^{\,2} + \vec{v}^2)^{\frac{1}{2}}$$

Equation 4:

$$Ca^{2+}\ Wave\ Direction = \arctan\left(\frac{\vec{u}}{\vec{v}}\right) \pm 180$$

Equations 1 and 2 calculate vector components ($\vec{u}$ and $\vec{v}$) using vector magnitude (u_i - assigned an arbitrary value of 1) and wave direction in degrees (θ_i). Equation 3 calculates the average vector magnitude (Ca^{2+} Polarity Score) using the mean $\vec{u}$ and $\vec{v}$ for all of the Ca^{2+} waves measured

in a single MK. Equation 4 calculates the mean Ca^{2+} Wave Direction using mean $\vec{u}$ and $\vec{v}$, where

180° is added if $\arctan\left(\frac{\vec{u}}{\vec{v}}\right)$ is < 180 and 180° is subtracted if $\arctan\left(\frac{\vec{u}}{\vec{v}}\right) > 180$.

Fibrinogen polarity was quantified by first identifying the 120° sector of each MK that had developed the greatest fluorescence intensity 6 min after stimulation. The sum fluorescence intensity of this sector ($F_{sectmax}$) and the total fluorescence intensity of the entire MK (F_{WC}) were used to calculate the degree of fibrinogen polarity with Equation 5.

Equation 5:

$$Fibrinogen\ Polarity\ = \frac{F_{sectmax} \times 3}{F_{wc}} - 1$$

FRAP measurements

MKs were preincubated with 10 µM cytochalasin D or vehicle and then stimulated for 2 min with 100 µM ADPβS in the presence of 60 µg/ml Alexa Fluor 647–labelled fibrinogen. The labelled fibrinogen was then bleached by exposure to a 635-nm laser at maximum intensity for 300 ms within a 16-µm² circular region at the cell periphery. Recovery of fluorescence was monitored by confocal imaging (Olympus FV1000, see above) at a rate of 0.2 Hz for 220 s. Longer recordings could not be performed because this assay was particularly sensitive to the small movements of MKs that naturally occur over time. Data were analyzed with the following equation to correct for nonspecific bleaching and normalize to the pre-bleach and post-bleach fluorescence intensity values:

Equation 6:

$$Normalised\ Bx = \frac{\left(\frac{Bx - Bg}{Rx - Bg}\right) - \left(\frac{Bb - Bg}{Rb - Bg}\right)}{\left(\frac{Bi - Bg}{Ri - Bg}\right) - \left(\frac{Bb - Bg}{Rb - Bg}\right)}$$

where Bx is the fluorescence intensity of the bleached ROI at x s, Bb is the fluorescence intensity of the bleached ROI immediately after photobleaching, Bi is the initial fluorescence intensity of the bleached ROI at, Rx is the fluorescence intensity of the reference ROI (non-bleached region of the MK), Rb is the fluorescence intensity of the reference ROI immediately after photobleaching, Ri is the initial fluorescence intensity of the reference ROI, and Bg is the average fluorescence intensity of the background ROI.

Immunocytochemistry

MKs suspended in HBSS with 60 µg/ml Alexa Fluor 647–labelled fibrinogen were stimulated with 100 µM ADPβS for 6 min and then fixed in 8% formyl saline for 10 min. Cells were washed in HBSS, permeablized with 0.2% triton X-100 for 10 min, and then washed again in HBSS. Cells were blocked for 1 hour in 1% w/v bovine serum albumin (BSA) and stained for 1 hour with Alexa Fluor 488–conjugated phalloidin (1:1000) in 1% BSA. Cells were then washed three times in HBSS and imaged with a 60X objective lens on a Nikon F1000 confocal microscope.

Statistical analysis

Statistical testing was performed as described in the individual figure legends with GraphPad Prism software (La Jolla, Ca).

Supplementary Materials

Movie S1. Intracellular Ca^{2+} signaling and fibrinogen binding after stimulation with ADPβS.
Movie S2. Intracellular Ca^{2+} signaling and fibrinogen binding after stimulation with ionomycin.

References and Notes
1. B. Nieswandt, D. Varga-Szabo, M. Elvers, Integrins in platelet activation. *Journal of thrombosis and haemostasis : JTH* **7 Suppl 1**, 206-209 (2009); published online EpubJul (10.1111/j.1538-7836.2009.03370.x).
2. C. Kim, F. Ye, M. H. Ginsberg, Regulation of integrin activation. *Annu Rev Cell Dev Biol* **27**, 321-345 (2011)10.1146/annurev-cellbio-100109-104104).
3. L. Stefanini, R. C. Roden, W. Bergmeier, CalDAG-GEFI is at the nexus of calcium-dependent platelet activation. *Blood* **114**, 2506-2514 (2009); published online EpubSep 17 (10.1182/blood-2009-04-218768).
4. K. Eto, R. Murphy, S. W. Kerrigan, A. Bertoni, H. Stuhlmann, T. Nakano, A. D. Leavitt, S. J. Shattil, Megakaryocytes derived from embryonic stem cells implicate CalDAG-GEFI in integrin signaling. *Proc Natl Acad Sci U S A* **99**, 12819-12824 (2002); published online EpubOct 1 (10.1073/pnas.202380099).
5. L. Stefanini, D. S. Paul, R. F. Robledo, E. R. Chan, T. M. Getz, R. A. Campbell, D. O. Kechele, C. Casari, R. Piatt, K. M. Caron, N. Mackman, A. S. Weyrich, M. C. Parrott, Y. Boulaftali, M. D. Adams, L. L. Peters, W. Bergmeier, RASA3 is a critical inhibitor of RAP1-dependent platelet activation. *J Clin Invest* **125**, 1419-1432 (2015); published online EpubApr (10.1172/JCI77993).
6. L. Stefanini, W. Bergmeier, RAP1-GTPase signaling and platelet function. *J Mol Med (Berl)* **94**, 13-19 (2016); published online EpubJan (10.1007/s00109-015-1346-3).
7. A. M. Battram, T. N. Durrant, E. O. Agbani, K. J. Heesom, D. S. Paul, R. Piatt, A. W. Poole, P. J. Cullen, W. Bergmeier, S. F. Moore, I. Hers, The Phosphatidylinositol 3,4,5-trisphosphate (PI(3,4,5)P3) Binder Rasa3 Regulates Phosphoinositide 3-kinase (PI3K)-dependent Integrin alphaIIbbeta3 Outside-in Signaling. *J Biol Chem* **292**, 1691-1704 (2017); published online EpubFeb 3 (10.1074/jbc.M116.746867).
8. F. Lagarrigue, C. Kim, M. H. Ginsberg, The Rap1-RIAM-talin axis of integrin activation and blood cell function. *Blood* **128**, 479-487 (2016); published online EpubJul 28 (10.1182/blood-2015-12-638700).
9. G. Dupont, L. Combettes, G. S. Bird, J. W. Putney, Calcium oscillations. *Cold Spring Harbor perspectives in biology* **3**, (2011); published online EpubMar (10.1101/cshperspect.a004226).
10. A. B. Parekh, Decoding cytosolic Ca2+ oscillations. *Trends in biochemical sciences* **36**, 78-87 (2011); published online EpubFeb (10.1016/j.tibs.2010.07.013).
11. R. E. Dolmetsch, K. Xu, R. S. Lewis, Calcium oscillations increase the efficiency and specificity of gene expression. *Nature* **392**, 933-936 (1998); published online EpubApr 30 (10.1038/31960).
12. S. Wray, T. Burdyga, Sarcoplasmic reticulum function in smooth muscle. *Physiological reviews* **90**, 113-178 (2010); published online EpubJan (10.1152/physrev.00018.2008).
13. K. Machaca, Ca2+ signaling differentiation during oocyte maturation. *Journal of cellular physiology* **213**, 331-340 (2007); published online EpubNov (10.1002/jcp.21194).
14. A. H. Cornell-Bell, S. M. Finkbeiner, M. S. Cooper, S. J. Smith, Glutamate induces calcium waves in cultured astrocytes: long-range glial signaling. *Science* **247**, 470-473 (1990); published online EpubJan 26 (
15. M. J. Berridge, Inositol trisphosphate and calcium signalling mechanisms. *Biochimica et biophysica acta* **1793**, 933-940 (2009); published online EpubJun (10.1016/j.bbamcr.2008.10.005).

16. L. T. Izu, Y. Xie, D. Sato, T. Banyasz, Y. Chen-Izu, Ca(2)(+) waves in the heart. *Journal of molecular and cellular cardiology* **58**, 118-124 (2013); published online EpubMay (10.1016/j.yjmcc.2012.11.014).

17. J. W. Heemskerk, J. Hoyland, W. T. Mason, S. O. Sage, Spiking in cytosolic calcium concentration in single fibrinogen-bound fura-2-loaded human platelets. *Biochem J* **283 (Pt 2)**, 379-383 (1992); published online EpubApr 15 (

18. M. Mazzucato, M. R. Cozzi, M. Battiston, M. Jandrot-Perrus, M. Mongiat, P. Marchese, T. J. Kunicki, Z. M. Ruggeri, L. De Marco, Distinct spatio-temporal Ca2+ signaling elicited by integrin alpha2beta1 and glycoprotein VI under flow. *Blood* **114**, 2793-2801 (2009); published online EpubSep 24 (10.1182/blood-2008-12-193490).

19. S. I. Obydennyy, A. N. Sveshnikova, F. I. Ataullakhanov, M. A. Panteleev, Dynamics of calcium spiking, mitochondrial collapse and phosphatidylserine exposure in platelet subpopulations during activation. *Journal of thrombosis and haemostasis : JTH*, (2016); published online EpubJun 25 (10.1111/jth.13395).

20. N. N. Topalov, Y. N. Kotova, S. A. Vasil'ev, M. A. Panteleev, Identification of signal transduction pathways involved in the formation of platelet subpopulations upon activation. *British journal of haematology* **157**, 105-115 (2012); published online EpubApr (10.1111/j.1365-2141.2011.09021.x).

21. F. Ye, C. Kim, M. H. Ginsberg, Reconstruction of integrin activation. *Blood* **119**, 26-33 (2012); published online EpubJan 5 (10.1182/blood-2011-04-292128).

22. S. Tertyshnikova, A. Fein, [Ca2+]i oscillations and [Ca2+]i waves in rat megakaryocytes. *Cell calcium* **21**, 331-344 (1997); published online EpubMay (

23. D. Thomas, M. J. Mason, M. P. Mahaut-Smith, Depolarisation-evoked Ca2+ waves in the non-excitable rat megakaryocyte. *The Journal of physiology* **537**, 371-378 (2001); published online EpubDec 1 (

24. S. J. Shattil, A. D. Leavitt, All in the family: primary megakaryocytes for studies of platelet alphaIIbbeta3 signaling. *Thrombosis and haemostasis* **86**, 259-265 (2001); published online EpubJul (

25. G. Tolhurst, C. Vial, C. Leon, C. Gachet, R. J. Evans, M. P. Mahaut-Smith, Interplay between P2Y(1), P2Y(12), and P2X(1) receptors in the activation of megakaryocyte cation influx currents by ADP: evidence that the primary megakaryocyte represents a fully functional model of platelet P2 receptor signaling. *Blood* **106**, 1644-1651 (2005); published online EpubSep 1 (10.1182/blood-2005-02-0725).

26. S. Jones, R. J. Evans, M. P. Mahaut-Smith, Extracellular Ca(2+) modulates ADP-evoked aggregation through altered agonist degradation: implications for conditions used to study P2Y receptor activation. *British journal of haematology* **153**, 83-91 (2011); published online EpubApr (10.1111/j.1365-2141.2010.08499.x).

27. B. Z. Paul, J. L. Daniel, S. P. Kunapuli, Platelet shape change is mediated by both calcium-dependent and -independent signaling pathways. Role of p160 Rho-associated coiled-coil-containing protein kinase in platelet shape change. *J Biol Chem* **274**, 28293-28300 (1999); published online EpubOct 1 (

28. J. R. Crittenden, W. Bergmeier, Y. Zhang, C. L. Piffath, Y. Liang, D. D. Wagner, D. E. Housman, A. M. Graybiel, CalDAG-GEFI integrates signaling for platelet aggregation and thrombus formation. *Nature medicine* **10**, 982-986 (2004); published online EpubSep (10.1038/nm1098).

29. G. Hollopeter, H. M. Jantzen, D. Vincent, G. Li, L. England, V. Ramakrishnan, R. B. Yang, P. Nurden, A. Nurden, D. Julius, P. B. Conley, Identification of the platelet ADP receptor targeted by antithrombotic drugs. *Nature* **409**, 202-207 (2001); published online EpubJan 11 (10.1038/35051599).

30. J. M. Cosemans, I. C. Munnix, R. Wetzker, R. Heller, S. P. Jackson, J. W. Heemskerk, Continuous signaling via PI3K isoforms beta and gamma is required for platelet ADP receptor function in dynamic thrombus stabilization. *Blood* **108**, 3045-3052 (2006); published online EpubNov 1 (10.1182/blood-2006-03-006338).

31. J. E. Fabre, M. Nguyen, A. Latour, J. A. Keifer, L. P. Audoly, T. M. Coffman, B. H. Koller, Decreased platelet aggregation, increased bleeding time and resistance to thromboembolism in P2Y1-deficient mice. *Nature medicine* **5**, 1199-1202 (1999); published online EpubOct (10.1038/13522).

32. C. J. Foster, D. M. Prosser, J. M. Agans, Y. Zhai, M. D. Smith, J. E. Lachowicz, F. L. Zhang, E. Gustafson, F. J. Monsma, Jr., M. T. Wiekowski, S. J. Abbondanzo, D. N. Cook, M. L. Bayne, S. A. Lira, M. S. Chintala, Molecular identification and characterization of the platelet ADP receptor targeted by thienopyridine antithrombotic drugs. *The Journal of clinical investigation* **107**, 1591-1598 (2001); published online EpubJun (10.1172/JCI12242).

33. B. Hechler, A. Eckly, P. Ohlmann, J. P. Cazenave, C. Gachet, The P2Y1 receptor, necessary but not sufficient to support full ADP-induced platelet aggregation, is not the target of the drug clopidogrel. *British journal of haematology* **103**, 858-866 (1998); published online EpubDec (

34. J. Jin, S. P. Kunapuli, Coactivation of two different G protein-coupled receptors is essential for ADP-induced platelet aggregation. *Proceedings of the National Academy of Sciences of the United States of America* **95**, 8070-8074 (1998); published online EpubJul 7 (

35. C. Leon, B. Hechler, M. Freund, A. Eckly, C. Vial, P. Ohlmann, A. Dierich, M. LeMeur, J. P. Cazenave, C. Gachet, Defective platelet aggregation and increased resistance to thrombosis in purinergic P2Y(1) receptor-null mice. *The Journal of clinical investigation* **104**, 1731-1737 (1999); published online EpubDec (10.1172/JCI8399).

36. J. Jin, J. L. Daniel, S. P. Kunapuli, Molecular basis for ADP-induced platelet activation. II. The P2Y1 receptor mediates ADP-induced intracellular calcium mobilization and shape change in platelets. *J Biol Chem* **273**, 2030-2034 (1998); published online EpubJan 23 (

37. T. J. Hallam, T. J. Rink, Responses to adenosine diphosphate in human platelets loaded with the fluorescent calcium indicator quin2. *The Journal of physiology* **368**, 131-146 (1985); published online EpubNov (

38. S. J. Mundell, M. L. Jones, A. R. Hardy, J. F. Barton, S. M. Beaucourt, P. B. Conley, A. W. Poole, Distinct roles for protein kinase C isoforms in regulating platelet purinergic receptor function. *Molecular pharmacology* **70**, 1132-1142 (2006); published online EpubSep (10.1124/mol.106.023549).

39. A. R. Hardy, P. B. Conley, J. Luo, J. L. Benovic, A. W. Poole, S. J. Mundell, P2Y1 and P2Y12 receptors for ADP desensitize by distinct kinase-dependent mechanisms. *Blood* **105**, 3552-3560 (2005); published online EpubMay 1 (10.1182/blood-2004-07-2893).

40. S. O. Sage, E. H. Yamoah, J. W. Heemskerk, The roles of P(2X1)and P(2T AC)receptors in ADP-evoked calcium signalling in human platelets. *Cell calcium* **28**, 119-126 (2000); published online EpubAug (10.1054/ceca.2000.0139).

41. A. R. Hardy, M. L. Jones, S. J. Mundell, A. W. Poole, Reciprocal cross-talk between P2Y1 and P2Y12 receptors at the level of calcium signaling in human platelets. *Blood* **104**, 1745-1752 (2004); published online EpubSep 15 (10.1182/blood-2004-02-0534).

42. S. M. Schoenwaelder, A. Ono, S. Sturgeon, S. M. Chan, P. Mangin, M. J. Maxwell, S. Turnbull, M. Mulchandani, K. Anderson, G. Kauffenstein, G. W. Rewcastle, J. Kendall, C. Gachet, H. H. Salem, S. P. Jackson, Identification of a unique co-operative phosphoinositide 3-kinase signaling mechanism regulating integrin alpha IIb beta 3 adhesive function in platelets. *J Biol Chem* **282**, 28648-28658 (2007); published online EpubSep 28 (10.1074/jbc.M704358200).

43. D. Woulfe, H. Jiang, R. Mortensen, J. Yang, L. F. Brass, Activation of Rap1B by G(i) family members in platelets. *J Biol Chem* **277**, 23382-23390 (2002); published online EpubJun 28 (10.1074/jbc.M202212200).

44. G. F. Guidetti, I. Canobbio, M. Torti, PI3K/Akt in platelet integrin signaling and implications in thrombosis. *Adv Biol Regul* **59**, 36-52 (2015); published online EpubSep (10.1016/j.jbior.2015.06.001).

45. G. Kauffenstein, W. Bergmeier, A. Eckly, P. Ohlmann, C. Leon, J. P. Cazenave, B. Nieswandt, C. Gachet, The P2Y(12) receptor induces platelet aggregation through weak activation of the alpha(IIb)beta(3) integrin--a phosphoinositide 3-kinase-dependent mechanism. *FEBS letters* **505**, 281-290 (2001); published online EpubSep 14 (

46. J. L. Joyal, D. J. Burks, S. Pons, W. F. Matter, C. J. Vlahos, M. F. White, D. B. Sacks, Calmodulin activates phosphatidylinositol 3-kinase. *J Biol Chem* **272**, 28183-28186 (1997); published online EpubNov 7 (

47. W. Chen, I. Thielmann, S. Gupta, H. Subramanian, D. Stegner, R. van Kruchten, A. Dietrich, S. Gambaryan, J. W. Heemskerk, H. M. Hermanns, B. Nieswandt, A. Braun, Orai1-induced store-operated Ca(2+) entry enhances phospholipase activity and modulates canonical transient receptor potential channel 6 function in murine platelets. *Journal of thrombosis and haemostasis : JTH* **12**, 528-539 (2014); published online EpubApr (10.1111/jth.12525).

48. A. K. Rao, M. A. Kowalska, J. Disa, Impaired cytoplasmic ionized calcium mobilization in inherited platelet secretion defects. *Blood* **74**, 664-672 (1989); published online EpubAug 1 (

49. X. Yang, L. Sun, S. Ghosh, A. K. Rao, Human platelet signaling defect characterized by impaired production of inositol-1,4,5-triphosphate and phosphatidic acid and diminished Pleckstrin phosphorylation: evidence for defective phospholipase C activation. *Blood* **88**, 1676-1683 (1996); published online EpubSep 1 (

50. S. B. Lee, A. K. Rao, K. H. Lee, X. Yang, Y. S. Bae, S. G. Rhee, Decreased expression of phospholipase C-beta 2 isozyme in human platelets with impaired function. *Blood* **88**, 1684-1691 (1996); published online EpubSep 1 (

51. R. C. Liddington, M. H. Ginsberg, Integrin activation takes shape. *J Cell Biol* **158**, 833-839 (2002); published online EpubSep 2 (10.1083/jcb.200206011).

52. D. R. Critchley, Cytoskeletal proteins talin and vinculin in integrin-mediated adhesion. *Biochem Soc Trans* **32**, 831-836 (2004); published online EpubNov (10.1042/BST0320831).

53. S. Miyamoto, S. K. Akiyama, K. M. Yamada, Synergistic roles for receptor occupancy and aggregation in integrin transmembrane function. *Science* **267**, 883-885 (1995); published online EpubFeb 10 (

54. J. Zhu, C. V. Carman, M. Kim, M. Shimaoka, T. A. Springer, B. H. Luo, Requirement of alpha and beta subunit transmembrane helix separation for integrin outside-in signaling. *Blood* **110**, 2475-2483 (2007); published online EpubOct 1 (10.1182/blood-2007-03-080077).

55. C. Cluzel, F. Saltel, J. Lussi, F. Paulhe, B. A. Imhof, B. Wehrle-Haller, The mechanisms and dynamics of (alpha)v(beta)3 integrin clustering in living cells. *J Cell Biol* **171**, 383-392 (2005); published online EpubOct 24 (10.1083/jcb.200503017).

56. W. Li, J. Llopis, M. Whitney, G. Zlokarnik, R. Y. Tsien, Cell-permeant caged InsP3 ester shows that Ca2+ spike frequency can optimize gene expression. *Nature* **392**, 936-941 (1998); published online EpubApr 30 (10.1038/31965).

57. N. Pugh, B. D. Maddox, D. Bihan, K. A. Taylor, M. P. Mahaut-Smith, R. W. Farndale, Differential integrin activity mediated by platelet collagen receptor engagement under flow conditions. *Thrombosis and haemostasis* **117**, 1588-1600 (2017); published online EpubJul 26 (10.1160/TH16-12-0906).

58. W. S. Nesbitt, S. Kulkarni, S. Giuliano, I. Goncalves, S. M. Dopheide, C. L. Yap, I. S. Harper, H. H. Salem, S. P. Jackson, Distinct glycoprotein Ib/V/IX and integrin alpha IIbbeta 3-dependent calcium signals cooperatively regulate platelet adhesion under flow. *J Biol Chem* **277**, 2965-2972 (2002); published online EpubJan 25 (10.1074/jbc.M110070200).

59. J. W. Heemskerk, P. Vis, M. A. Feijge, J. Hoyland, W. T. Mason, S. O. Sage, Roles of phospholipase C and Ca(2+)-ATPase in calcium responses of single, fibrinogen-bound platelets. *J Biol Chem* **268**, 356-363 (1993); published online EpubJan 5 (

60. C. Uneyama, H. Uneyama, N. Akaike, Cytoplasmic Ca2+ oscillation in rat megakaryocytes evoked by a novel type of purinoceptor. *The Journal of physiology* **470**, 731-749 (1993); published online EpubOct (

61. M. Iino, Spatiotemporal dynamics of Ca2+ signaling and its physiological roles. *Proc Jpn Acad Ser B Phys Biol Sci* **86**, 244-256 (2010).

62. C. D. Lawson, K. Burridge, The on-off relationship of Rho and Rac during integrin-mediated adhesion and cell migration. *Small GTPases* **5**, e27958 (2014)10.4161/sgtp.27958).

63. F. Moheimani, D. E. Jackson, P2Y12 receptor: platelet thrombus formation and medical interventions. *Int J Hematol* **96**, 572-587 (2012); published online EpubNov (10.1007/s12185-012-1188-5).

64. G. Berger, R. Quarck, D. Tenza, S. Levy-Toledano, J. de Gunzburg, E. M. Cramer, Ultrastructural localization of the small GTP-binding protein Rap1 in human platelets and megakaryocytes. *British journal of haematology* **88**, 372-382 (1994); published online EpubOct (

65. K. Nagata, Y. Nozawa, A low M(r) GTP-binding protein, Rap1, in human platelets: localization, translocation and phosphorylation by cyclic AMP-dependent protein kinase. *British journal of haematology* **90**, 180-186 (1995); published online EpubMay (

66. M. J. Caloca, J. L. Zugaza, M. Vicente-Manzanares, F. Sanchez-Madrid, X. R. Bustelo, F-actin-dependent translocation of the Rap1 GDP/GTP exchange factor RasGRP2. *J Biol Chem* **279**, 20435-20446 (2004); published online EpubMay 7 (10.1074/jbc.M313013200).

67. J. Clyde-Smith, G. Silins, M. Gartside, S. Grimmond, M. Etheridge, A. Apolloni, N. Hayward, J. F. Hancock, Characterization of RasGRP2, a plasma membrane-targeted, dual specificity Ras/Rap exchange factor. *J Biol Chem* **275**, 32260-32267 (2000); published online EpubOct 13 (10.1074/jbc.M006087200).

68. M. C. Beckerle, D. E. Miller, M. E. Bertagnolli, S. J. Locke, Activation-dependent redistribution of the adhesion plaque protein, talin, in intact human platelets. *The Journal of cell biology* **109**, 3333-3346 (1989); published online EpubDec (

69. B. Franke, J. W. Akkerman, J. L. Bos, Rapid Ca2+-mediated activation of Rap1 in human platelets. *EMBO J* **16**, 252-259 (1997); published online EpubJan 15 (10.1093/emboj/16.2.252).

70. M. J. Berridge, M. D. Bootman, P. Lipp, Calcium--a life and death signal. *Nature* **395**, 645-648 (1998); published online EpubOct 15 (10.1038/27094).

71. P. Nicotera, S. Orrenius, The role of calcium in apoptosis. *Cell calcium* **23**, 173-180 (1998); published online EpubFeb-Mar (

72. K. Irie, A. Masuda, M. Shindo, Y. Nakagawa, H. Ohigashi, Tumor promoter binding of the protein kinase C C1 homology domain peptides of RasGRPs, chimaerins, and Unc13s. *Bioorg Med Chem* **12**, 4575-4583 (2004); published online EpubSep 1 (10.1016/j.bmc.2004.07.008).

73. J. E. Johnson, R. E. Goulding, Z. Ding, A. Partovi, K. V. Anthony, N. Beaulieu, G. Tazmini, R. B. Cornell, R. J. Kay, Differential membrane binding and diacylglycerol recognition by C1 domains of RasGRPs. *Biochem J* **406**, 223-236 (2007); published online EpubSep 1 (10.1042/BJ20070294).

74. C. W. Taylor, S. C. Tovey, IP(3) receptors: toward understanding their activation. *Cold Spring Harbor perspectives in biology* **2**, a004010 (2010); published online EpubDec (10.1101/cshperspect.a004010).

75. M. Spindler, J. M. M. van Eeuwijk, Y. Schurr, P. Nurden, B. Nieswandt, D. Stegner, A. Reinhold, M. Bender, ADAP deficiency impairs megakaryocyte polarization with ectopic proplatelet release and causes microthrombocytopenia. *Blood* **132**, 635-646 (2018); published online EpubAug 9 (10.1182/blood-2018-01-829259).

76. S. Dutting, F. Gaits-Iacovoni, D. Stegner, M. Popp, A. Antkowiak, J. M. M. van Eeuwijk, P. Nurden, S. Stritt, T. Heib, K. Aurbach, O. Angay, D. Cherpokova, N. Heinz, A. A. Baig, M. G. Gorelashvili, F. Gerner, K. G. Heinze, J. Ware, G. Krohne, Z. M. Ruggeri, A. T. Nurden, H. Schulze, U. Modlich, I. Pleines, C. Brakebusch, B. Nieswandt, A Cdc42/RhoA regulatory circuit downstream of glycoprotein Ib guides transendothelial platelet biogenesis. *Nat Commun* **8**, 15838 (2017); published online EpubJun 15 (10.1038/ncomms15838).

77. L. Stefanini, R. H. Lee, D. S. Paul, E. C. O'Shaughnessy, D. Ghalloussi, C. I. Jones, Y. Boulaftali, K. O. Poe, R. Piatt, D. O. Kechele, K. M. Caron, K. M. Hahn, J. M. Gibbins, W. Bergmeier, Functional redundancy between RAP1 isoforms in murine platelet production and function. *Blood*, (2018); published online EpubAug 21 (10.1182/blood-2018-03-838714).

78. M. P. Mahaut-Smith, D. Thomas, A. B. Higham, J. A. Usher-Smith, J. F. Hussain, J. Martinez-Pinna, J. N. Skepper, M. J. Mason, Properties of the demarcation membrane system in living rat megakaryocytes. *Biophysical journal* **84**, 2646-2654 (2003); published online EpubApr (10.1016/S0006-3495(03)75070-X).

79. S. K. Grange, "Technical note: Averaging wind speeds and directions (Research gate technical report)," (Research Gate, 2014).

Fig. 1. Integrin $\alpha_{IIb}\beta_3$ activation is dependent upon the timing and magnitude of ADPβS-evoked, repetitive Ca^{2+} transients. (**A** to **F**) Characteristics of the $[Ca^{2+}]_i$ transients and fibrinogen accumulation as measured by confocal fluorescence microscopy analysis of primary rat MKs after stimulation with ADPβS at the indicated times. Whole-cell images (A) and fluorescence traces (B to D) of the cytoplasmic Ca^{2+} concentration (blue) and peripheral fibrinogen binding (red) are representative of six independent experiments performed in duplicate. Fibrinogen binding events were quantified in terms of the peak increase (Peak ΔF) and net change (Net ΔF). (E and

F) Linear regression analysis of quantified maximal fibrinogen-binding events (Peak ΔF) versus Peak Ca^{2+} F/F_0 (E) or the net change in fibrinogen binding (Net ΔF) versus Ca^{2+} Transient Interval (F). Relationships for individual experiments are shown by the gray lines and the average of all experiments is indicated by the red line. *$P < 0.05$ by Pearson correlation.

Fig. 2. Rapid activation of integrin $\alpha_{IIb}\beta_3$ is dependent on synergy between P2Y1 and P2Y12 receptors. (**A** to **I**) Confocal fluorescence microscopy analysis of $[Ca^{2+}]_i$ transients and fibrinogen accumulation in primary rat MKs after stimulation with ADPβS (A to F) or ionomycin (G to I) over the indicated times. Responses are representative of at least three independent experiments. The blue traces represent the whole-cell intracellular Ca^{2+} responses and the red traces represent peripheral fibrinogen binding. (D) The cumulative integrated Ca^{2+} increase (green) alongside Ca^{2+} and fibrinogen responses during the initial four Ca^{2+} transients of the experiment shown in (A). (A to D) Responses to ADPβS were compared after cytoplasmic loading with the Ca^{2+} chelator BAPTA (C), incubation with the P2Y1 antagonist MRS2179 (E), incubation with the P2Y12 antagonist Cangrelor (F), or exposure to vehicle as a control (B). (H and I) Responses to ionomycin after incubation with vehicle (H) compared to responses to ionomycin and ADPβS when MKs had been treated with MRS2179 (I). (**J**) Quantification of the mean lag period between the onset of $[Ca^{2+}]_i$ flux and fibrinogen binding in response to ADPβS or ionomycin with or without MRS2179 or Cangrelor. Data are means ± SD of at least three independent experiments. ***$P < 0.001$ by one-way ANOVA with Tukey's multiple comparisons test; n.s., not significant; n/a, not applicable due to complete inhibition.

Fig. 3. Enhanced [Ca²⁺]ᵢ and activation of PI3K are required for rapid αᵢᵢᵦβ₃ activation. (A to K) Confocal fluorescence microscopy analysis of [Ca²⁺]ᵢ transients and fibrinogen accumulation in primary rat MKs after stimulation with ADPβS (A to G) or ionomycin (I to K). Intracellular Ca²⁺ (blue) and fibrinogen binding (red) responses are representative of at least three independent experiments for ADPβS (A to G) and ionomycin (I to K). Cells were treated with vehicle (A) or the specified inhibitors U73122 (B and J), U73343 (C and K), GF109203 (D), LY294002 (E and I) SQ22536 (F), or a combination of SQ22536 and Cangrelor (G). For the control ionomycin-evoked response, see Fig. 2G. (H) Peak increase in fibrinogen in response to ADPβS for all cells in each of the conditions shown in (A) to (G); n ≥ 3 for each condition; bar shows the mean ± SD. *$P < 0.05$ by one-way ANOVA with Dunn's multiple comparisons test.

Fig. 4. Directional polarity of P2Y receptor–evoked Ca²⁺ waves in MKs. (A to F) Spatial analysis of ADPβS-evoked transient [Ca²⁺]ᵢ waves in primary rat MKs. (A to C) Confocal fluorescence images showing the progression of a single [Ca²⁺]ᵢ wave (A) or 10 consecutive waves (B and D). (A) Left: The octants used to calculate radar plots and Ca²⁺ wave score are displayed in the pre-stimulus image. The progression of a Ca²⁺ wave is shown by the dotted red lines in subsequent images at the stated time after stimulation. (B and D) The red arrows depict the direction of travel of individual waves, whereas a dotted circle represents Ca²⁺ increases that lacked a clear direction of travel across the cell. The extent to which all waves within a single cell displayed a net polarity is summarized within radar plots based upon the percentage of [Ca²⁺]ᵢ waves travelling towards each octant (C andE). (B and C) Images and analysis of an MK with a low polarity score. (D and E)

Images and analysis of an MK with a high Ca^{2+} polarity score. (F) Quantification of the Ca^{2+} polarity score calculated for 12 MKs measured in seven independent experiments.

Fig. 5. Development of a polarized integrin $\alpha_{IIb}\beta_3$ distribution after stimulation by ADPβS, but not ionomycin. (**A** to **D**) Confocal fluorescence microscopy analysis of fibrinogen binding to primary rat MKs after stimulation with ADPβS or ionomycin. Fluorescence intensity radar plots (top) and confocal images (bottom) of surface-bound fibrinogen in a single MK before and at 2-min intervals after stimulation with ADPβS (A) or ionomycin (B). (C) Quantification of the fibrinogen polarity score against time after stimulation with ADPβS [red line corresponding to the cell shown in (A)] or ionomycin [blue line corresponding to the cell shown in (B)]. (D) A scatter plot comparing fibrinogen polarity scores calculated 6 min after stimulation with ADPβS (n = 12) or ionomycin (n = 10). Data are means ± SD; *$P < 0.05$ by Students t test. The cells selected in (A) and (C) show representative data from an MK with a high polarity score after stimulation with ADPβS (n = 6) and all MKs after treatment with ionomycin (n = 10).

Fig. 6. Ca^{2+} wave direction coordinates the polarization of activated integrin $\alpha_{IIb}\beta_3$. (**A** to **G**) Confocal fluorescence microscopy and analysis of the relationship between $[Ca^{2+}]_i$ waves and fibrinogen binding in primary rat MKs after stimulation with ADPβS. (A to C) Representative cell showing low polarity scores for both Ca^{2+} wave direction and fibrinogen binding. (D to F) Representative of a cell with high polarity scores for both parameters. Radar plot analysis (A, B, D, and E) of Ca^{2+} wave direction (A and D) and fibrinogen binding (B and D) together with fluorescence images of fibrinogen binding (C and F) before and every 2 min after stimulation. (G)

Linear regression analysis of fibrinogen polarity score against Ca^{2+} polarity score for 12 MKs, which gave a statistically significant non-zero fit ($P < 0.05$) with a positive gradient (0.59). (**H**) Schematic diagram representing the difference in angle between the average point of origin of Ca^{2+} waves and the center of fibrinogen polarity in 5 MKs that had a fibrinogen polarity score > 0.5.

Fig. 7. The mobility and distribution of activated $\alpha_{IIb}\beta_3$ in the plasma membrane are dependent on its association with the actin cytoskeleton. (**A** to **C**) FRAP analysis of fibrinogen bound to ADPβS-stimulated MKs as measured by confocal fluorescence microscopy. (A) Images of fibrinogen bound to an ADPβS-stimulated MK before and immediately after bleaching of a defined region (dotted circle) at the cell periphery. (B) Normalized fluorescence recovery over time within the bleached region after treatment with vehicle (black line) or cytochalasin D (red line). The responses are representative of six independent experiments. (C) Average maximum recovery of fluorescence within the bleached region after 4 min. Data are means ± SEM of six independent experiments. (**D** to **G**) Confocal fluorescence analysis of fibrinogen binding (red) and actin (green) in MKs fixed 4 min after stimulation with ADPβS. Data are representative of an MK with either a low (D and E) or a high (F and G) fibrinogen polarity score, taken from three independent experiments. (D and F) Seven consecutive fluorescence images at 1-μm intervals from a z-stack and with a 3D reconstruction of the whole MK (right panel). (E and G) Radar plots of normalized fluorescence intensity for fibrinogen and actin around the circumference of the MKs for each confocal slice. *$P < 0.05$ by Students t test.
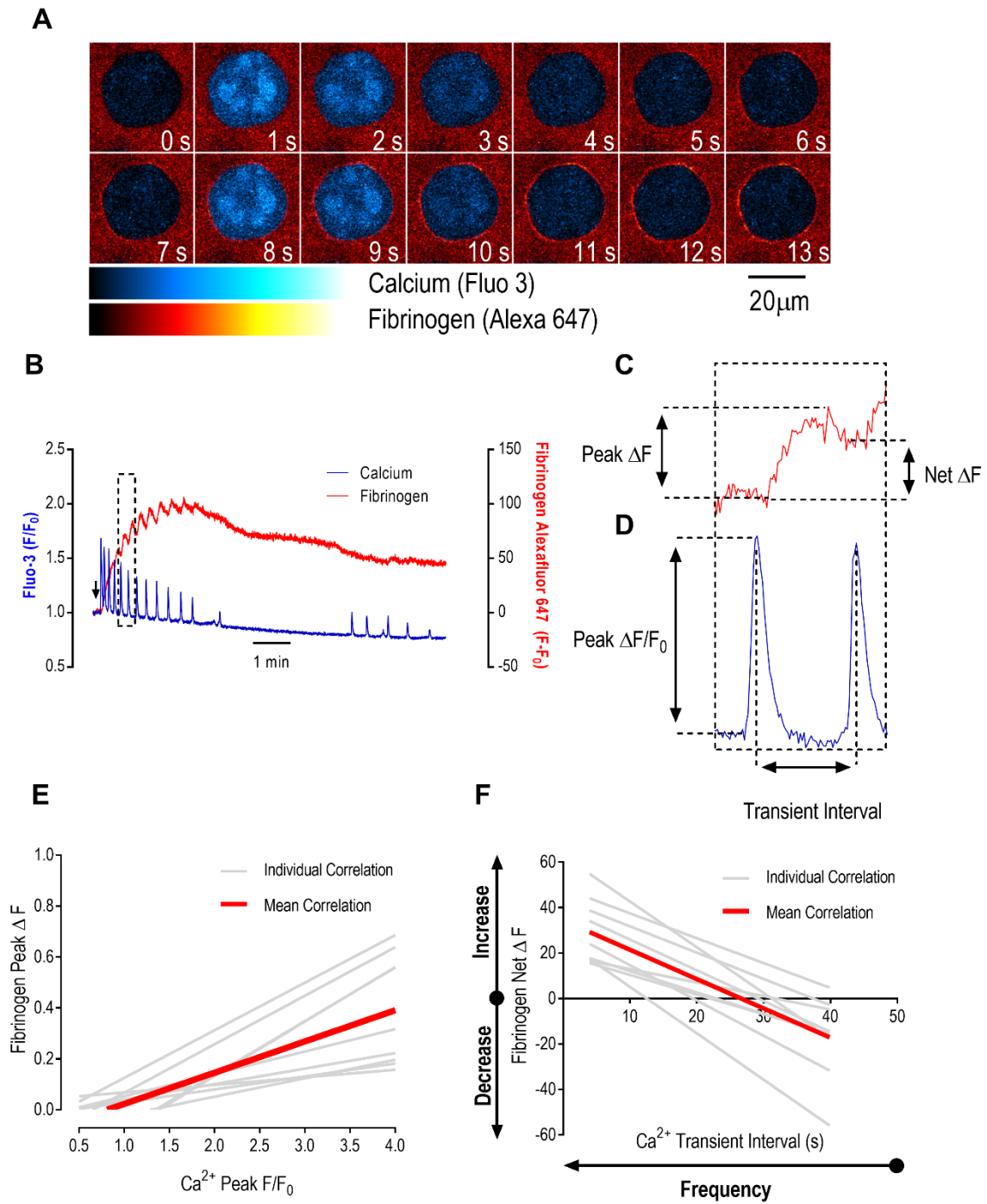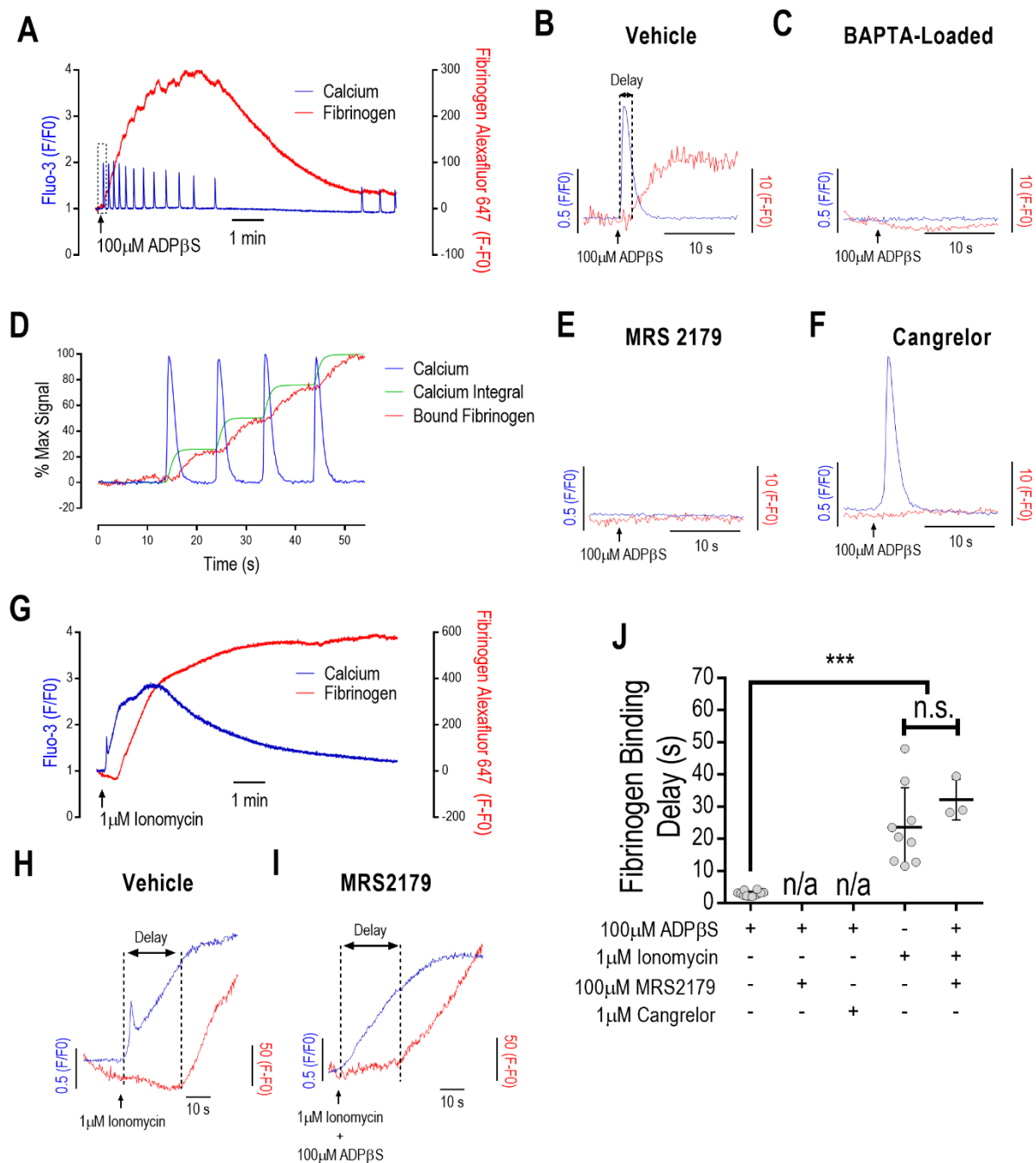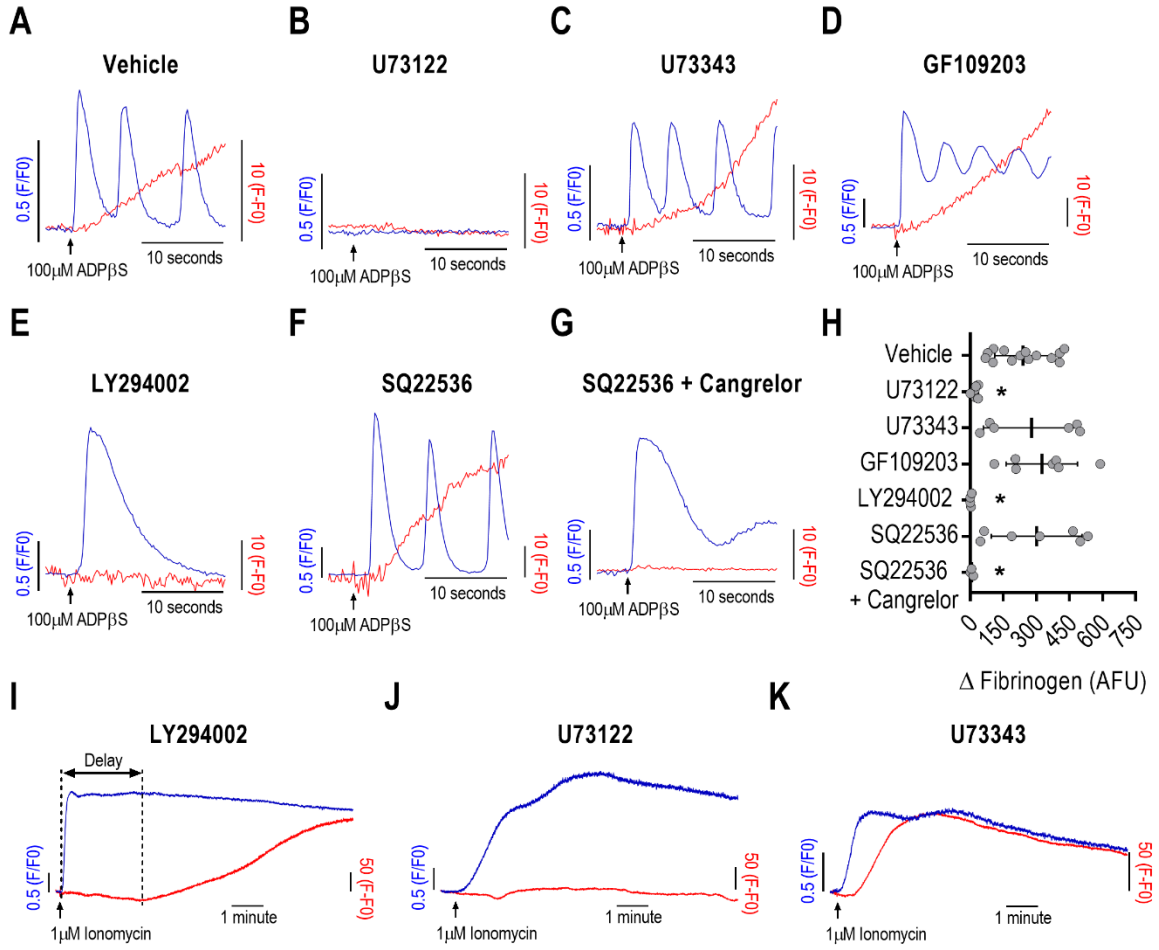
Figure 1

A

Calcium (Fluo 3)
Fibrinogen (Alexa 647)

20μm

B

C

Peak ΔF

Net ΔF

D

Peak ΔF/F$_0$

Transient Interval

E

F

Figure 2

A

Fluo-3 (F/F0) | Fibrinogen Alexafluor 647 (F-F0)

- Calcium
- Fibrinogen

100μM ADPβS   1 min

B Vehicle

Delay

0.5 (F/F0) | 10 (F-F0)

100μM ADPβS   10 s

C BAPTA-Loaded

0.5 (F/F0) | 10 (F-F0)

100μM ADPβS   10 s

D

% Max Signal

- Calcium
- Calcium Integral
- Bound Fibrinogen

Time (s)

E MRS 2179

0.5 (F/F0) | 10 (F-F0)

100μM ADPβS   10 s

F Cangrelor

0.5 (F/F0) | 10 (F-F0)

100μM ADPβS   10 s

G

Fluo-3 (F/F0) | Fibrinogen Alexafluor 647 (F-F0)

- Calcium
- Fibrinogen

1μM Ionomycin   1 min

H Vehicle

Delay

0.5 (F/F0) | 50 (F-F0)

1μM Ionomycin   10 s

I MRS2179

Delay

0.5 (F/F0) | 50 (F-F0)

1μM Ionomycin + 100μM ADPβS   10 s

J

Fibrinogen Binding Delay (s)

*** | n.s.

n/a n/a

100μM ADPβS	+	+	+	−	+
1μM Ionomycin	−	−	−	+	+
100μM MRS2179	−	+	−	−	+
1μM Cangrelor	−	−	+	−	−

Figure 3

A Vehicle

B U73122

C U73343

D GF109203

0.5 (F/F0)   10 (F-F0)   100μM ADPβS   10 seconds

E LY294002

F SQ22536

G SQ22536 + Cangrelor

0.5 (F/F0)   10 (F-F0)   100μM ADPβS   10 seconds

H

Vehicle
U73122   *
U73343
GF109203
LY294002   *
SQ22536
SQ22536
+ Cangrelor   *

0 150 300 450 600 750

Δ Fibrinogen (AFU)

I LY294002

Delay

0.5 (F/F0)   50 (F-F0)   1μM Ionomycin   1 minute

J U73122

0.5 (F/F0)   50 (F-F0)   1μM Ionomycin   1 minute

K U73343

0.5 (F/F0)   50 (F-F0)   1μM Ionomycin   1 minute

Figure 4

A

0 ms   188 ms   376 ms   564 ms   752 ms

8 µm

B

Low Ca²⁺ Polarity Score

C

D

High Ca²⁺ Polarity Score

E

F

Ca²⁺ Polarity Score

ADPβS

Figure 5

A

100µM ADPβS

B

1µM Ionomycin

0 min   2 min   4 min   6 min   8 min

8 µm

C

ADPβS
Ionomycin

Fibrinogen Polarity Score

Time (m)

D

Fibrinogen Polarity Score

*

ADPβS   Ionomycin

Figure 6

Low Ca²⁺ Polarity Score

High Ca²⁺ Polarity Score

0 min   2 min   4 min   6 min   8 min

8 µm

Figure 7

A

Before   After

8µm

B

10µM Cytochalasin D
Control

C

Max Recovery

*

Vehicle
10µM Cyt D

D

8µm

E

F

G